PROCEEDINGS OF SCIENCE

$\bar{K}$ and η nuclear quasi-bound states

Jiří Mareš*
Nuclear Physics Institute, 250 68 Řež, Czech Republic
E-mail: mares@ujf.cas.cz

Recent studies of K^- and η nuclear quasi-bound states are reviewed. The $\bar{K}N$ and ηN scattering amplitudes used in the calculations are constructed within coupled-channel models that capture the physics of the $\Lambda(1405)$ and $N^*(1535)$ resonances, respectively. The role played by the strong energy dependence of the scattering amplitudes near threshold and the implications of self-consistenct treatment are discussed.

52 International Winter Meeting on Nuclear Physics - Bormio 2014,
27-31 January 2014
Bormio, Italy

*Speaker.

© Copyright owned by the author(s) under the terms of the Creative Commons Attribution-NonCommercial-ShareAlike Licence.

PoS(Bormio 2014)046

1. Introduction

The study of interactions of antikaons and η mesons with nucleons and the nuclear medium has been attracting considerable attention in last years (see [1, 2, 3, 4, 5] and references therein), and yet, the issue as well as the closely related problem of K^- and η nuclear bound states is far from being resolved. The near-threshold $\bar{K}N$ and ηN attraction generated by the $\Lambda(1405)$ and $N^*(1535)$ resonances, respectively, appear to be strong enough to allow binding of the K^- and η meson in nuclei, however, in-medium modifications and energy dependence of the underlying scattering amplitudes have to be carefully taken into account in relevant calculations.

The present contribution concerns systematic treatments of energy and density dependences within dynamical and self consistent calculations of K^- and η bound states in nuclei (more details can be found in Refs. [6, 7, 4, 5]).

In Section 2, we briefly discuss in-medium modifications of the $\bar{K}N$ and ηN scattering amplitudes, construct the self energy operator and demonstrate how to incorporate the strong energy and density dependence of the scattering amplitudes at and near threshold in the calculations of mesic nuclei. In Section 3, we summarize current status of calculations of few-body kaonic clusters and present selected results of our dynamical self-consistent calculations of K^- nuclear states in heavier nuclei. Section 4 is devoted to an overview of our recent study of η nuclear bound states and brief summary is given in Section 5.

2. Energy and density dependence of in-medium amplitudes

The near-threshold $\bar{K}N$ and ηN scattering amplitudes are both attractive and strongly energy dependent in models that generate dynamically the nearby meson-baryon s-wave resonances $\Lambda(1405)$ and $N^*(1535)$, respectively.

Current calculations of K^--nuclear quasi-bound states are often based on the $\bar{K}N$ interactions derived within an SU(3) chiral approach combined with coupled channel T-matrix resummation techniques [8, 9, 10]. The meson-baryon channels considered in this approach include $\pi\Lambda$, $\pi\Sigma$, $\bar{K}N$, $\eta\Lambda$, $\eta\Sigma$, and $K\Xi$. Free parameters of the models are fitted to threshold and low-energy K^-p data. The $\Lambda(1405)$ resonance is generated dynamically and its presence induces strong energy dependence in the scattering amplitudes $F_{\bar{K}N}(\sqrt{s})$.

The chirally-inspired coupled-channel ηN interaction can be constructed in a close analogy with the $\bar{K}N$ case [5]. Here, the relevant meson-baryon channels include $I = 1/2$ states πN, ηN, $K\Lambda$, $K\Sigma$, and $I = 3/2$ states πN and $K\Sigma$. Free parameters of the model are fitted to $\pi N \to \pi N$ amplitudes for the $S11$ and $S31$ partial waves (SAID database [11]) and selected $\pi N \to \eta N$ cross section data.

In our calculations we often applied meson-baryon coupled-channel separable s-wave interactions by Cieplý and Smejkal [10, 12, 13] which are matched to equivalent chiral SU(3) scattering amplitudes derived from the chiral effective Lagrangian at up to next-to-leading order (NLO). While the basic features of the $\bar{K}N$ interactions are satisfactorily described already by the leading order (LO) Tomozawa-Weinberg term, a good reproduction of the πN and ηN data requires NLO contributions since the relevant data involve dominantly the πN channel which is decoupled from the ηN channel at LO.

PoS(Bormio 2014)046

Solving the coupled-channel Lippmann-Schwinger equations $F = V + VGF$ with the potential kernels leads to a separable form of in-medium scattering amplitudes F_{ij}, given in the two-body cm system by

$$F_{ij}(k,k';\sqrt{s},\rho) = g_i(k^2)\, f_{ij}(\sqrt{s},\rho)\, g_j(k'^2)\ . \tag{2.1}$$

Here, $g_j(k^2)$ is a momentum-space form factor, j runs over channels, and in-medium reduced amplitudes $f_{ij}(\sqrt{s},\rho)$ are expressed as

$$f_{ij}(\sqrt{s},\rho) = \left[(1 - v(\sqrt{s})\cdot G(\sqrt{s},\rho))^{-1}\cdot v(\sqrt{s})\right]_{ij}\ , \tag{2.2}$$

where G is an intermediate state meson-baryon Green's function:

$$G_n(\sqrt{s},\rho) = -4\pi \int_{\Omega_n(\rho)} \frac{d^3p}{(2\pi)^3} \frac{g_n^2(p^2)}{k_n^2 - p^2 - \Pi^{(n)}(\sqrt{s},\rho) + \mathrm{i}0}\ . \tag{2.3}$$

The integration domain $\Omega_n(\rho)$ is limited by the Pauli principle in channels n involving nucleon. The self-energy $\Pi^{(n)}(\sqrt{s},\rho)$ stands for the sum of hadron self-energies in channel n. (The self-energies are discussed in detail in Ref. [5]). In particular, the meson (h) self-energy $\Pi_h^{(hN)} = (E_N/\sqrt{s})\Pi_h$ in the diagonal $n \equiv (hN)$ channel, where the lab self-energy Π_h is given by

$$\Pi_h(\sqrt{s},\rho) \equiv 2\omega_h V_h = -\frac{\sqrt{s}}{E_N} 4\pi F_{hN}(\sqrt{s},\rho)\rho\ , \tag{2.4}$$

depending implicitly on $\omega_h = m_h - B_h$ and on the off-shell two-body momenta k, k'. This self-energy serves as input in Eq. 2.3 and therefore also in Eq. 2.2 and Eq. 2.1 for the output scattering amplitude, requires by Eq. 2.4 the knowledge of the same scattering amplitude. This calls for a self-consistent calculation of the in-medium scattering amplitudes.

Several amplitudes used in our calculations of η nuclear states – denoted GW [14] and M2 (also M1) [15] – are available only in free-space forms. Therefore, appropriate in-medium versions accounting fo Pauli blocking have been produced in Ref. [4] by applying the Ericson-Ericson multiple-scattering approach [16]:

$$F_{\eta N}(\sqrt{s},\rho) = \frac{F_{\eta N}(\sqrt{s})}{1 + \xi(\rho)(\sqrt{s}/m_N)F_{\eta N}(\sqrt{s})\rho}\ , \tag{2.5}$$

where

$$\xi(\rho) = \frac{9\pi}{4p_F^2} I(\kappa),\ \ I(\kappa) = 4\int_0^\infty \frac{dt}{t}\exp(-\kappa t)\, j_1^2(t)\ . \tag{2.6}$$

where $p_F = (3\pi^2\rho/2)^{1/3}$ is the local Fermi momentum corresponding to density ρ and $\xi(\rho)$ accounts for Pauli blocking. These in-medium amplitudes were then used as input within self-consistent calculations.

In-medium $\bar{K}N$ and ηN amplitudes near threshold are shown in Fig. 1 and Fig. 2, respectively. Free space amplitudes are presented for comparison. The typical strong energy dependence shown in the figures is a consequence of the nearby resonances $\Lambda(1405)$ and $N^*(1535)$.

Figure 1 shows the in-medium reduced scattering amplitudes $f_{KN}(\sqrt{s},\rho) = 1/2[f_{K^-p}(\sqrt{s},\rho) + f_{K^-n}(\sqrt{s},\rho)]$ as function of $\sqrt{s}$ for nuclear matter density $\rho_0 = 0.17$ fm^{-3}, corresponding to the

PoS(Bormio 2014)046

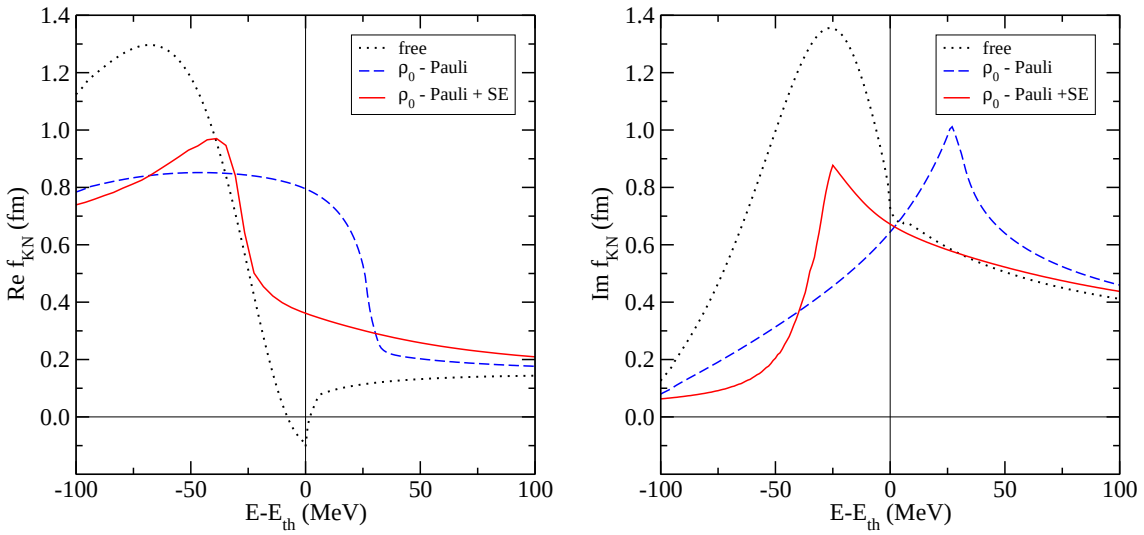

Figure 1: Energy dependence of the c.m. reduced amplitude f_{KN} in the NLO30 model [12] (left: real part, right: imaginary part). Dotted line: free space; dashed line: Pauli blocked amplitude for $\rho_0 = 0.17$ fm^{-3}; solid line: including also hadron self-energies ('+SE') at ρ_0. The thin vertical line denotes the $K^- p$ threshold.

interaction of the K^- meson with symmetric nuclear matter. The amplitudes were calculated using two in-medium versions, with and without hadron self energies. The pronounced energy dependence of the scattering amplitude appears crucial in the self-consistent calculations of kaonic nuclear states. In particular, the real part of the '+SE' amplitude changes from weak attraction at and above threshold to strong attraction below threshold at energies relevant for self-consistent calculations of kaonic nuclei.

The nuclear medium effect on the energy dependence of the ηN scattering amplitude is demonstrated in Fig. 2. The peak structure observed in the figure for Im$F_{\eta N}$ may be ascribed to the $N^*(1535)$ resonance generated dynamically in the coupled-channel model. In-medium Pauli blocking shifts the resonance to higher energies, making it more pronounced. Implementing hadron self-energies spreads the resonance structure over a broad interval of energies, practically dissolving it in the nuclear medium. This behavior is different from that observed for the $\bar{K}N$ system where the hadron self-energies compensate to large extent for the effect of Pauli blocking and bring the peak structure back below the $\bar{K}N$ threshold (see Fig. 1). This results in strong in-medium attraction with little energy dependence at subthreshold energies relevant for K^--nuclear bound states [17]. In contrast, the in-medium ηN amplitudes decrease substantially upon going below threshold and are weaker than the respective free-space amplitudes. In particular, the relatively large value of the free-space Re$a_{\eta N}$ is almost halved for nuclear matter density. This implies that K^- bound states are very likely to exist, whereas η nuclear states may not bind. Similarly, the widths generated by the imaginary part of the scattering amplitudes are considerably larger for K^- than for η mesons.

It is to be stressed that the scattering amplitudes are highly model dependent. The $\bar{K}N$ amplitudes calculated within various models are usually close to each other at and above threshold and differ, often significantly, in the subthreshold region. On the other hand, the ηN scattering

PoS(Bormio 2014)046

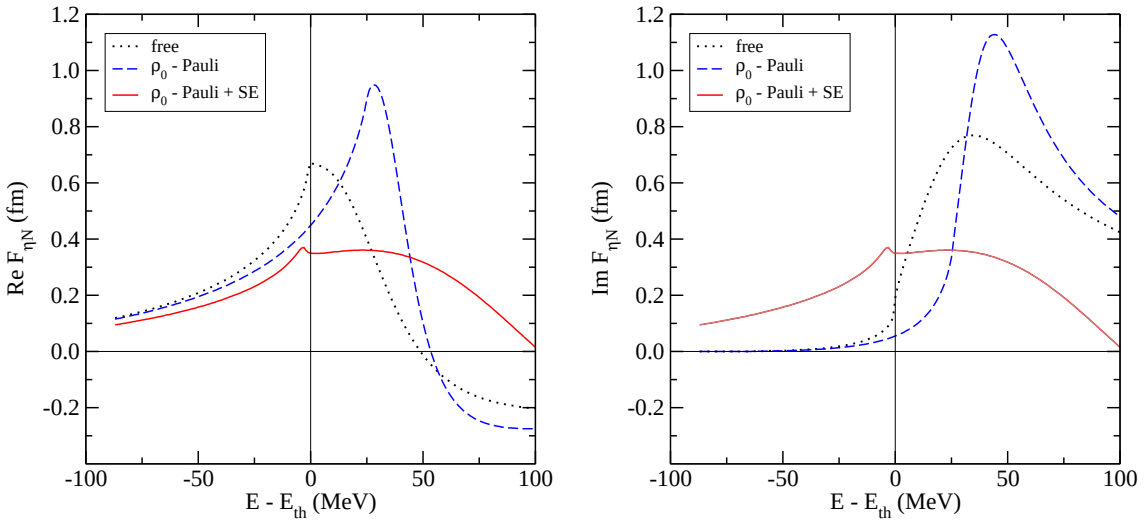

Figure 2: Energy dependence of the c.m. scattering amplitude $F_{\eta N}$ in the CS model [13, 5] (left: real part, right: imaginary part). Dotted line: free space; dashed line: Pauli blocked amplitude for $\rho_0 = 0.17$ fm^{-3}; solid line: including also hadron self-energies ('+SE') at ρ_0. The thin vertical line denotes the ηN threshold.

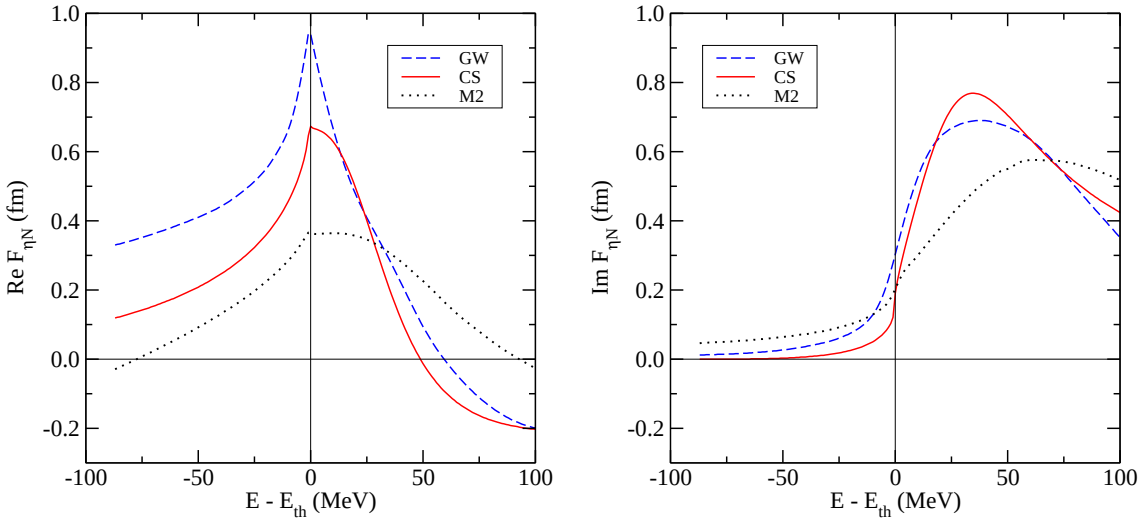

Figure 3: Real (left panel) and imaginary (right panel) parts of the ηN cm scattering amplitude $F_{\eta N}(\sqrt{s})$ as a function of the total cm energy $\sqrt{s}$ in three meson-baryon interaction models: dashed, GW [14]; solid, CS [13]; dotted, M2 [15]. The thin vertical line denotes the ηN threshold.

amplitudes differ below as well as above the ηN threshold, with perhaps just one common value $a_{\eta N} \approx 0.2 - 0.3$ fm for the imaginary part at threshold. This is illustrated in Fig. 3 for three different meson-baryon interaction models, GW [14], CS [13], and M1 [15].

The strong energy dependence in the scattering amplitudes $F_{\bar{K}N}(\sqrt{s})$ and $F_{\eta N}(\sqrt{s})$ has to be treated self-consistently, as shown in refs. [17, 18, 4]. The point is that in the nuclear medium (for

PoS(Bormio 2014)046

$A \gg 1$ approximated by the lab system) the argument $\sqrt{s}$ in the scattering amplitudes is given by

$$\sqrt{s} = \sqrt{(\sqrt{s_{\rm th}} - B_K - B_N)^2 - (\vec{p}_K + \vec{p}_N)^2} \leq \sqrt{s_{\rm th}}, \tag{2.7}$$

where $\sqrt{s_{\rm th}} \equiv m_h + m_N$ and B_h and B_N are meson and nucleon binding energies, and the momentum dependent term generates additional substantial downward energy shift, since $(\vec{p}_K + \vec{p}_N)^2 \neq 0$ unlike the case of the two-body cm system.

To leading order in binding energies and kinetic energies with respect to rest masses, the downward energy shift $\delta\sqrt{s} \equiv \sqrt{s} - \sqrt{s_{\rm th}}$ is expressed as

$$\delta\sqrt{s} \approx -B_N - B_h - \xi_N \frac{p_N^2}{2m_N} - \xi_h \frac{p_h^2}{2m_h} \,, \tag{2.8}$$

where $\xi_{N(h)} \equiv m_{N(h)}/(m_N + m_h)$. Using the Fermi Gas model for nucleons and the local density approximation, one gets

$$\delta\sqrt{s} \approx -B_N \frac{\rho}{\bar{\rho}} - \xi_N B_h \frac{\rho}{\rho_0} - \xi_N T_N (\frac{\rho}{\rho_0})^{2/3} - \xi_h \frac{\sqrt{s}}{\omega_h E_N} 2\pi {\rm Re}\, F_{hN}(\sqrt{s},\rho)\rho \,, \tag{2.9}$$

where $T_N = 23.0$ MeV at nuclear-matter density ρ_0, $B_N \approx 8.5$ MeV is an average nucleon binding energy and $\bar{\rho}$ is the average nuclear density. Expression (2.9) respects the low-density limit, $\delta\sqrt{s} \to 0$ upon $\rho \to 0$. For attractive scattering amplitudes, all four terms in Eq. (2.9) are negative definite, the last one providing substantial downward energy shift. Since $\sqrt{s}$ depends on Re $F_{hN}(\sqrt{s},\rho)$ which by itself depends on $\sqrt{s}$, it is clear that for a given value of B_h, $F_{hN}(\sqrt{s},\rho)$ has to be determined *self-consistently* by iterating Eq. (2.9). This is done at each radial point where ρ is given, and for each B_h value during the calculation of bound states.

3. K^- nuclear quasi-bound states

3.1 Few-body systems

The issue of the K^-pp quasi-bound state has been attracting considerable interest of theorists as well as experimentalists for more than a decade [19, 20, 21, 22, 23, 24, 25]. Yet, it is still far from being resolved. Table 1 summarizes the current status of calculations of K^-pp which stands for $\bar{K}NN$ with isospin $I = 1/2$ and spin-parity $J^\pi = 0^-$, dominated by $I_{NN} = 1$.

The calculations can be devided into two classes: variational calculations (denoted V in the table) where the complex $\bar{K}N$ interaction accounts for the $\bar{K}N$–$\pi\Sigma$ two-body coupled channels but

Table 1: Binding energies B and widths Γ of K^-pp calculated within variational (V) and Faddeev (F) approaches (in MeV).

	chiral, energy dependent			phenomenological, static calculations			
	V [26]	V [28]	F [27]	V [19]	F [20]	F [21]	V [23]
B	16	17–23	9–16	48	50–70	60–95	40–80
Γ	41	40–70	34–46	61	90–110	45–80	40–85

PoS(Bormio 2014)046

disregards $\bar{K}NN$–$\pi\Sigma N$ coupling, and coupled channels genuine three-body Faddeev calculations (F). The table illustrates that the method of solving the 3-body problem (variational or Faddeev) is less important that the choice of the underlying interaction model. The K^-pp binding energies calculated using chiral, energy dependent interactions (grouped in the left part of the table) are considerably lower than those calculated using phenomenological, energy independent interactions (in the right part of the table). It is a consequence of the substantial difference between the $(\bar{K}N)_{I=0}$ interaction strengths which yield a quasibound state at ≈1420 MeV in the former case and at ≈1405 MeV in the latter case.

Recently, Barnea et al. [26] performed calculations of three-body $(\bar{K}NN)_{I=1/2}$ (shown for $J^\pi = 0^-$ in Table 1) and four-body $(\bar{K}NNN)_{I=0,1}$ and $(\bar{K}\bar{K}NN)_{I=0}$ nuclear quasi-bound states. The $\bar{K}$-nuclear cluster wavefunctions were expanded in a hyperspherical basis and the ground-state binding energies were calculated variationally. The corresponding $\bar{K}N \to \pi Y$ widths were evaluated using the expression:

$$\frac{\Gamma}{2} \approx \langle \Psi_{g.s.} | -\mathrm{Im} V_{\bar{K}N} | \Psi_{g.s.} \rangle \,, \tag{3.1}$$

where $V_{\bar{K}N}$ sums overall pairwise $\bar{K}N$ interactions. For two-body interactions involved, the AV4' V_{NN} [29] was used together with an effective energy-dependent $V_{\bar{K}N}$ [22] and a weakly repulsive $V_{\bar{K}\bar{K}}$ [30]. In $\bar{K}$-nuclear clusters, the energy dependent $V_{\bar{K}N}(\sqrt{s})$ was evaluated self-consistently for $\sqrt{s}$, expressed near threshold in the form:

$$\sqrt{s} = \sqrt{s_{\mathrm{th}}} - \frac{B}{A} - \frac{A-1}{A} B_K - \xi_N \frac{A-1}{A} \langle T_{NN} \rangle - \xi_K \left(\frac{A-1}{A} \right)^2 \langle T_K \rangle \,, \tag{3.2}$$

where $\xi_{N(K)} = m_N(K)/(m_N + m_K)$, B is the total binding energy of the system, T_K is the kaon kinetic energy operator in the total cm frame and T_{NN} is the pairwise NN kinetic energy operator in the NN pair cm system. A similar procedure was used for the $\bar{K}\bar{K}NN$ cluster (see [26] for details).

Results of the self-consistent calculations by Barnea et al. are summarized in Fig. 4. Since $\bar{K}N$ amplitudes (and consequently potentials) decrease upon going subthreshold, self-consistent calcu-

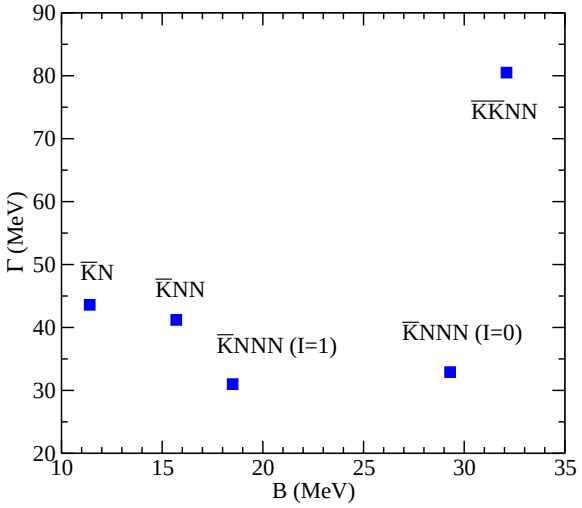

Figure 4: Calculated binding energies and $\bar{K}N \to \pi Y$ widths of few-body $\bar{K}$-nuclear clusters [26].

PoS(Bormio 2014)046

lations yield binding energies and widths of the calculated nuclear clusters lower than calculations performed at threshold, typically $\Delta B \sim 10$ MeV and $\Delta\Gamma \sim 10-40$ MeV. The results of K^-pp calculations are in agreement with the previous calculations using chiral energy-dependent $\bar{K}N$ amplitudes [28] (see also Table 1). In view of the low K^-pp binding energy $B(K^-pp) \approx 16$ MeV and relatively large absorption width $\Gamma(K^-pp) \approx 40$ MeV, it might be difficult to identify the K^-pp quasi-bound state unambiguously in ongoing experiments.

Relatively modest binding was found for the four-body $\bar{K}$ nuclear clusters, about 30 MeV in the lowest $I = 0$ systems, with absorption widths ranging from 30 MeV for $\bar{K}NNN$ to about 80 MeV for the $\bar{K}\bar{K}NN$ quasi-bound state.

It is to be noted that the widths shown in Fig. 4 are due to $\bar{K}N \to \pi Y$ decays only. Two-nucleon $K^-NN \to YN$ absorption widths are expected to contribute additional $\Delta\Gamma \lesssim 10$ MeV in $\bar{K}NN_{I=1/2}$ system [28] and ~ 20 MeV in the 4-body clusters [26]. The binding energies of K^- nuclear clusters could also be enhanced by dispersive contributions. Our recent fits to kaonic atoms [31, 32] suggest that $\Delta B_{\rm disp} \sim \Delta\Gamma_{\rm abs}$, and the binding energies could reach values $B(K^-pp) \sim 25$ MeV and $B(\bar{K}NNN,\ \bar{K}\bar{K}NN) \sim 50$ MeV.

3.2 Many-body systems

K^- nuclear quasi-bound states in many-body systems, as well as η nuclear quasi-bound states in Section 4, were calculated within the RMF formalism (see Refs. [17, 18] for details). The interaction of a meson (K^- or η) with a nucleus is described by the Klein–Gordon (KG) equation of the form

$$[\,\nabla^2 + \tilde{\omega}_h^2 - m_h^2 - \Pi_h(\omega_h,\rho)\,]\,\psi = 0\,, \tag{3.3}$$

where $\tilde{\omega}_h = \omega_h - {\rm i}\Gamma_h/2$ is complex energy of meson (in the case of antikaon containing also the Coulomb interaction), $\omega_h = m_h - B_h$, with B_h and Γ_h the binding energy and the width of the meson-nuclear bound state, respectively. The self-energy operator (discussed in Section 2) is constructed self-consistently within a chirally motivated coupled-channel model, using the RMF density distributions in a core nucleus.

We note that the potential V_h and the meson binding energy B_h appear as arguments in the expression for $\delta\sqrt{s}$ (Eq.(2.9)), which in turn serves as an argument for the self energy Π_h, and thus for V_h. Therefore, a self-consistency scheme in terms of both V_K and B_K is required for solving the KG equation (3.3).

In K^- nuclear calculations presented here, we considered two in-medium versions of the scattering amplitudes: the version which takes into account only Pauli blocking in the intermediate states, and the version (+SE) which adds self-consistently hadron in-medium self-energies (see Section 2). The $\bar{K}N$ amplitudes were constructed using the in-medium coupled-channel separable interaction model NLO30 [12] that reproduces all available low energy $\bar{K}N$ observables, including the latest $1s$ level shift and width in the K^- hydrogen atom from the SIDDHARTA experiment [33]. While the two in-medium versions of the $\bar{K}N$ scattering amplitudes yield by factor 2 different potential depths ${\rm Re}V_K$ at threshold, they give similar depths in the self-consistent calculations with the subthreshold extrapolation, ${\rm Re}V_K \sim 80-120$ MeV, depending on a particular nucleus.

The role of the self-consistent evaluation of the energy dependence of the $\bar{K}N$ scattering amplitude – and consequently of the potential V_K – is illustrated in Fig. 5. Here, the K^- nuclear

PoS(Bormio 2014)046

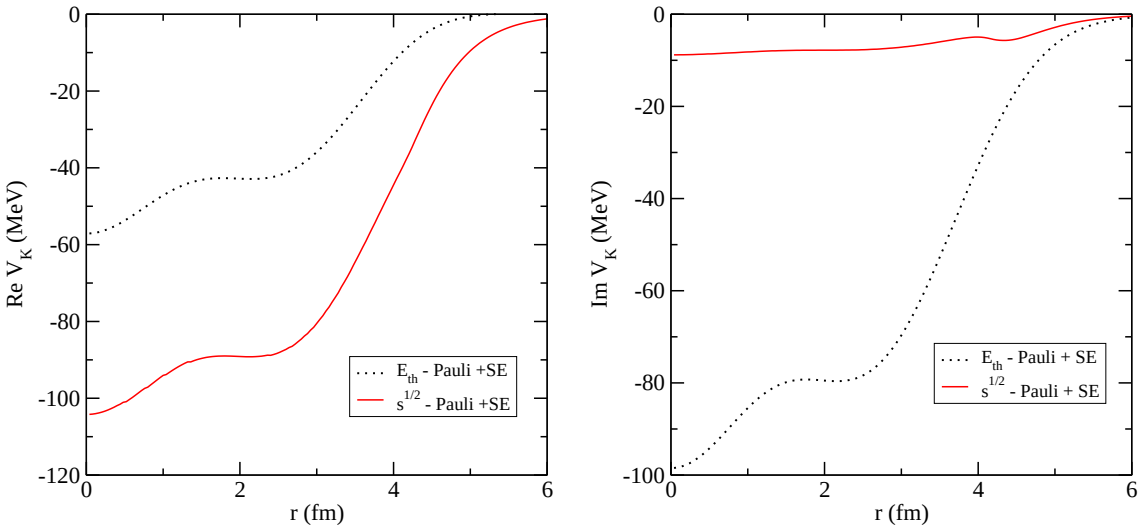

Figure 5: K^- nuclear potentials in Ca (left: real part, right: imaginary part), calculated with static RMF nuclear densities and chiral NLO30 amplitudes at threshold ('$E_{\rm th}$') and with $\delta\sqrt{s}$ (Eq. 2.9), in the in-medium version including self-energies ('+SE').

potential for $1s$ state in Ca at threshold ('$E_{\rm th}$') calculated using the '+SE' $\bar{K}N$ amplitude is compared with the potential for the energy shift $\delta\sqrt{s}$, evaluated self-consistently according to Eq.(2.9). The subthreshold extrapolation of $\sqrt{s}$ is clearly crucial for the depth of ReV_K, calculated using the '+SE' amplitude. The depth of ReV_K at threshold is about half of the self-consistently evaluated potential depth of Re$V_K(\sqrt{s})$. The imaginary parts of V_K, representing only $K^-N \to \pi Y$ decays, are considerably reduced in the self-consistent calculations, thus reflecting the proximity of the $\pi\Sigma$ threshold.

Figure 6 summarizes binding energies and widths of K^- quasi-bound states – including excited states – in selected nuclei calculated self-consistently for $\delta\sqrt{s}$ of Eq. 2.9, using the '+SE' amplitudes. The widths of low-lying K^- states due to $K^-N \to \pi Y$ conversions are substantially reduced in the self-consistent calculations as a result of the considerable energy shift $\delta\sqrt{s}$ towards the $\pi\Sigma$ threshold. On the contrary, the widths of higher excited K^- states are quite large even if only the pion conversion modes on a single nucleon are considered.

Finaly, Table 2 shows binding energies B_K and widths Γ_K of the $1s$ K^- nuclear quasi-bound states in O and Pb, calculated using the '+SE' scattering amplitudes. The results of fully dynamical RMF calculations which take into account the polarization of the nuclear core by the strongly bound K^- meson, are compared with the static RMF scheme in the first 2 blocks. It is to be stressed that the present chiral model of K^-–nucleus interaction does not account for the absorption of K^- mesons in the nuclear medium through non-pionic conversion modes on two nucleons $K^-NN \to YN$ ($Y = \Lambda, \Sigma$). To estimate the contribution of two-nucleon absorption processes to the decay widths of K^- nuclear states we introduced phenomenological term into the K^- self-energy:

$$\mathrm{Im}\,\Pi_K^{(2N)} = 0.2 f_{YN}(B_K) W_0 \rho^2, \tag{3.4}$$

where W_0 was fixed by kaonic atom data analysis and $f_{YN}(B_K)$ is kinematical suppression factor

PoS(Bormio 2014)046

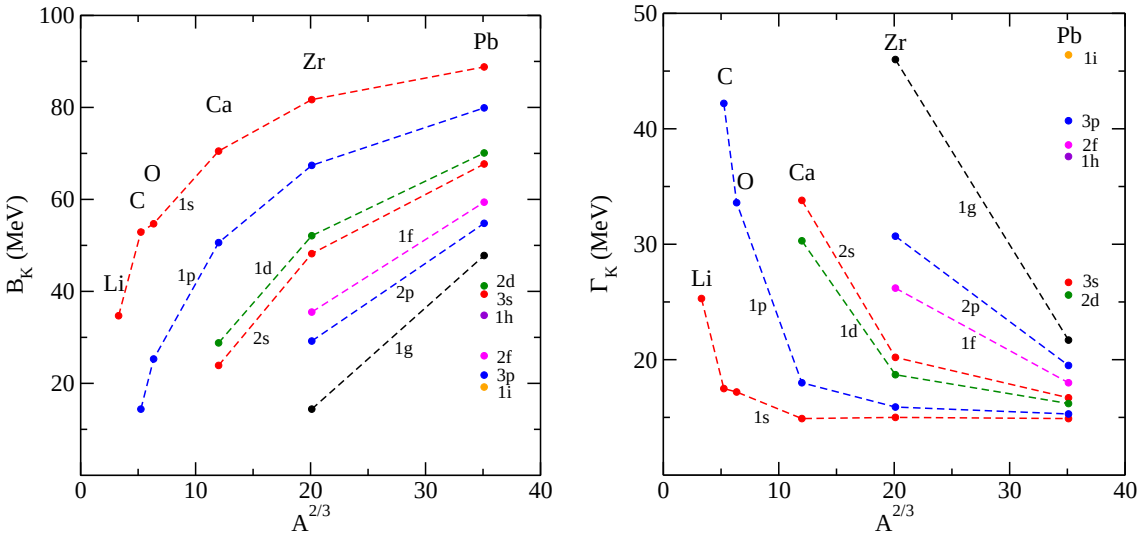

Figure 6: Binding energies B_K (left panel) and widths Γ_K (right panel) of K^- quasi-bound states in selected nuclei, calculated self-consistently with static RMF densities and the '+ SE' NLO30 scattering amplitudes. $K^-NN \to YN$ decay modes are not included.

taking into account reduced phase space available for decay products of K^- nuclear bound states [34]. When phenomenological terms are included to account for $2N$ absorption processes $\bar{K}NN \to YN$, the absorption widths $\Gamma_K \sim 50$ MeV become comparable to the binding energies B_K for *all* K^- nuclear quasi-bound states, exceeding considerably the level spacing. Our results should thus discourage attempts to search for isolated peaks corresponding to K^- nuclear quasi-bound states in many-body nuclear systems.

Table 2: Binding energies B_K and widths Γ_K (in MeV) of the $1s$ K^- nuclear quasi-bound states in O and Pb, calculated self-consistently using NLO30 '+SE' amplitudes. Dynamical and static RMF schemes are compared in the first two blocks and phenomenological $\bar{K}NN \to YN$ decay modes are included in the last block ('+2N abs.').

	dynamical		static		static + $2N$ abs.	
	B_K	Γ_K	B_K	Γ_K	B_K	Γ_K
O	54.7	17.2	57.8	16.4	53.7	46.4
Pb	88.8	14.9	89.1	14.8	88.0	55.3

4. η nuclear quasi-bound states

Free-space near-threshold ηN scattering amplitudes $F_{\eta N}(\sqrt{s})$ are highly model dependent, as was shown in Fig. 3 for three selected amplitude models (GW, CS, and M2). This model dependence manifests itself in the calculations of η nuclear quasi-bound states. In Fig.7, we present binding energies B_η and widths Γ_η calculated for $1s_\eta$ nuclear states in core nuclei from ^{12}C to ^{208}Pb using five representative ηN amplitude models, namely M1, M2 [15], GR [35], CS [13], and

PoS(Bormio 2014)046

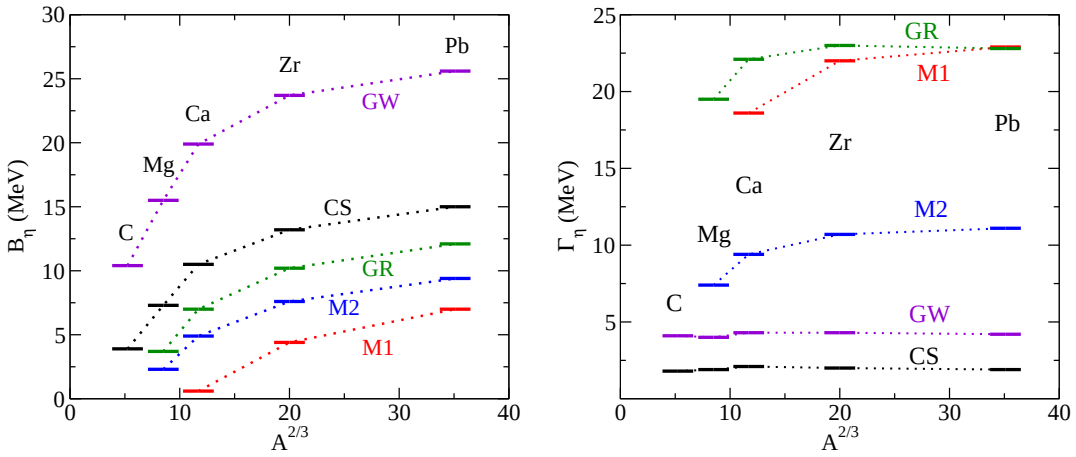

Figure 7: Binding energies (left) and widths (right) of $1s_\eta$ nuclear states across the periodic table calculated self consistently using the M1, M2 and GW subthreshold ηN scattering amplitudes within a dynamical RMF scheme, see text.

GW [14]. RMF equations of motion, along with the KG equation (3.3), are solved self consistently [4], thereby allowing for core polarization by the η meson. It si to be noted that the core polarization effect on B_η and Γ_η was found in all cases displayed here to be less than 1 MeV. The use of static nuclear densities is thus acceptable for not-too-light nuclear cores.

The left panel of Fig. 7 demonstrates that for each of the input ηN amplitude models the binding energy increases with A and tends to saturate for large values of A. The hierarchy of the curves reflects the strength of the Re$F_{\eta N}(\sqrt{s})$ input in the subthreshold region (compare Fig. 3). The M1 and M2 amplitudes are too weak to produce the $1s_\eta$ bound state in ^{12}C; the onset of binding for the weaker M1 amplitude is shifted to around ^{40}Ca. This illustrates the effect of the suppression of Re$F_{\eta N}(\sqrt{s})$ due to self-consistent treatment of its energy dependence. Namely, the M1 amplitude is the closest one on shell to the Haider-Liu amplitude [36] which was used by these authors to argue for ^{12}C as the approximate onset of η nuclear binding. In contrast, Re$F_{\eta N}(\sqrt{s})$ of the GW model is sufficiently strong to bind the $1s_\eta$ state in ^{12}C and even in lighter core nuclei, in spite of the suppression it undergoes here by forming its in-medium version and dealing with its energy dependence. The GW amplitude model admits the $1s_\eta$ bound state in ^{4}He with a binding energy of 1.2 MeV and a width of 2.3 MeV, both calculated using a static ^{4}He density.

The right panel of Fig. 7 shows substantial differences between the absorption widths Γ_η calculated using the above mentioned models. Here, the CS and GW model produce relatively small widths of order 2 and 4 MeV, respectively, uniformly across the periodic table. On the other hand, the other models give much larger widths which increase with A. Particularly the M1 and GR models predict widths of order 20 MeV. This reflects partly the energy dependence of Im$F_{\eta N}(\sqrt{s})$ in the subthreshold region, which is quite distinct in each one of the amplitude models, and partly the difference in the in-medium renormalization arising from the Re$F_{\eta N}(\sqrt{s})$ input. For instance, the large value of subthreshold downward energy shift due to the GW subthreshold amplitude (57 MeV at ρ_0 vs. 37 MeV in the M1 model) causes a particularly large reduction in the strength of the Im$F_{\eta N}(\sqrt{s})$ input for the GW amplitude model.

PoS(Bormio 2014)046

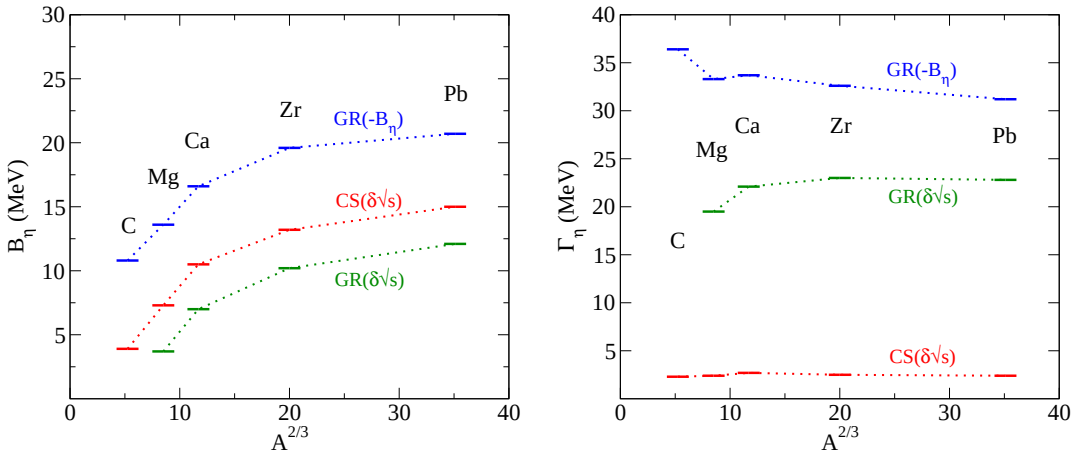

Figure 8: Binding energies (left) and widths (right) of $1s_\eta$ nuclear states across the periodic table calculated using the CS and GR ηN scattering amplitudes with different procedures for subthreshold energy shift $\delta\sqrt{s}$.

In order to illustrate the role of the energy dependence of the ηN scattering amplitudes in self-consistent evaluations of η nuclear states, it is instructive to apply our self-consistency scheme, based on $\delta\sqrt{s}$ of Eq. (2.9), to the GR in-medium energy- and density-dependent ηN interaction, and to compare the results with those obtained by GR using a density-independent $\delta\sqrt{s} = -B_\eta$ self-consistency requirement applied in Ref. [35]. This comparison is made in Fig. 8 where the in-medium CS model results are also included using Eq. (2.9) for subthreshold energy values for comparison (marked $\delta\sqrt{s}$ in the figure). The left and right panels exhibit $1s_\eta$-nuclear binding energies and widths, respectively. All calculations in the figure include self-energies and coupled-channels evaluation of Pauli blocking.

Comparing binding-energy and width results obtained by applying different self-consistency procedures in Fig. 8, one sees that our $\delta\sqrt{s}$ scheme (Eq. (2.9)) reduces considerably the GR binding energies and widths with respect to the original calculations of Ref. [35] that used a $\delta\sqrt{s} = -B_\eta$ procedure. However, even the reduced GR widths are still quite high, 20 MeV and over, suggesting that η-nuclear states will be extremely difficult to resolve if the GR model is the physically correct one.

Considering the CS results one again notes the remarkable smallness of the calculated widths shown on the right panel of Fig. 8, with values about 2 MeV (see also Fig. 7). It is to be noted that the widths calculated here do not include contributions from two-nucleon processes which are estimated to add a few MeV. We therefore anticipate that $1s_\eta$ and, wherever bound, also $1p_\eta$ nuclear states could in principle be observed if the CS model turns out to prove a realistic one.

Finally, in Fig. 9 we compare η-nuclear single-particle spectra across the periodic table evaluated self-consistently using two in-medium models, GW [14] (left panel) and CS [13] (right panel). These dynamical calculations include Pauli blocking, using Eqs. (2.5) and (2.6) for GW, and the coupled-channel approach discussed in Sect. 2 for CS. The latter model also incorporates in-medium hadron self-energies, resulting in 2–3 MeV lower binding energies. The widths calculated in both models are remarkably small (see Fig. 7). For these two models η-nuclear single-particle bound states have a chance of being observed, provided a suitable production/formation reaction

PoS(Bormio 2014)046

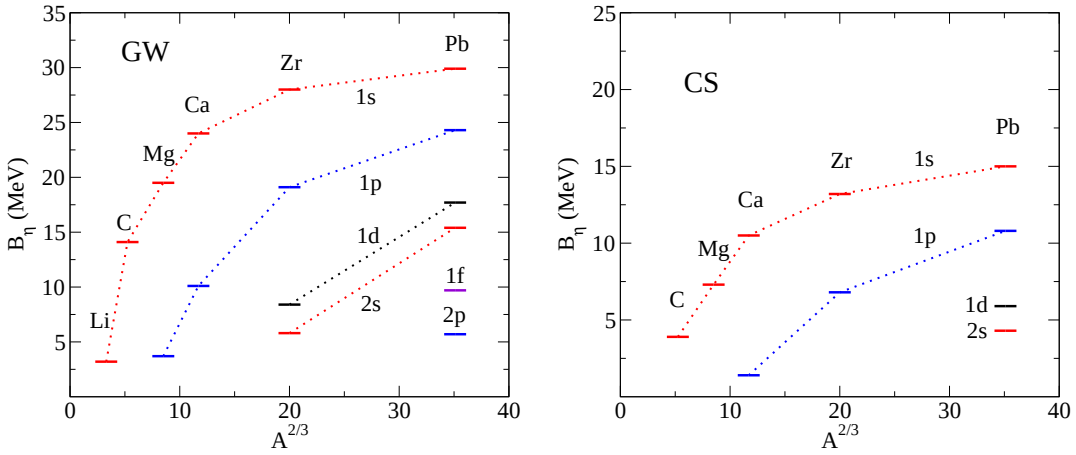

Figure 9: Binding energies (left) and widths (right) of $1s_\eta$ nuclear states across the periodic table calculated self consistently using the M1, M2 and GW subthreshold ηN scattering amplitudes within a dynamical RMF scheme.

is found. Other models studied by us produce either too large widths or are too weak to generate η-nuclear bound states over a substantial range of the periodic table.

5. Conclusions

In this contribution, we presented our recent self-consistent calculations of K^-- and η- nuclear quasi-bound states using scattering amplitudes constructed within meson-baryon coupled-channel (mostly chirally - inspired) models. We focused on the role played by the underlying meson-baryon subthreshold dynamics. We demonstrated how the energy dependence of the meson-nucleon in-medium scattering amplitudes transforms into density dependence of the meson self-energies.

Self-consistent calculations of K^- nuclear states yield sizable K^- absorption widths which are comparable or even larger than the corresponding binding energies. This suggests that an unambiguous identification of such quasi-bound states in ongoing experiments would be an extremely difficult task.

The in-medium subthreshold ηN amplitudes relevant for calculations of η nuclear bound states are substantially weaker than the ηN scattering length. The relatively large downward energy shift in our self-consistent approach leads to bound state energies and widths which are considerably smaller than those evaluated in comparable models. The small widths calculated in the CS and GW models might encourage further experimental searches for η nuclear bound states. However, the small widths, as well well as the values of the binding energies are strongly model dependent – other models predict substantially larger widths. To date, the only claim of observing an η nuclear bound state is in the reaction $p + {}^{27}\mathrm{Al} \rightarrow {}^{3}\mathrm{He} + {}^{25}_{\eta}\mathrm{Mg} \rightarrow {}^{3}\mathrm{He} + p + \pi^- + X$ reported recently by the COSY-GEM collaboration [37].

PoS(Bormio 2014)046

Acknowledgements

I wish to thank my colleagues Aleš Cieplý, Eli Friedman, Avraham Gal, and Daniel Gazda.
This work was supported by the GACR Grant No. 203/12/2126, as well as by the EU initiative FP7, HadronPhysics3, under the SPHERE and LEANNIS cooperation programs.

References

[1] See contributions in: A. Gal, R. S. Hayano (Eds.), *Recent Advances in Strangeness Nuclear Physics*, Nucl. Phys. A 804 (2008) 171-348.

[2] See contributions in: B. F. Gibson, K. Imai, T. Motoba, T. Nagae, A. Ohnishi (Eds.), *Proc. 10th Int. Conf. on Hypernuclear and Strange Particle Physics*, Tokai, 14-18 September 2009, Nucl. Phys. A 835 (2010) 1-469.

[3] See contributions in: B. Julia-Diaz, V Magas, E. Oset, A. Parreno, L. Tolos, I. Vidana, A. Ramos (Eds.), *Proc. 11th Int. Conf. on Hypernuclear and Strange Particle Physics*, Barcelona, 1 - 5 October 2012, Nucl. Phys. A 914 (2012) 1-568.

[4] E. Friedman, A. Gal, J. Mareš, Phys. Lett. B 725 (2013) 334.

[5] A. Cieplý, E. Friedman, A. Gal, J. Mareš, Nucl. Phys. A 925 (2014) 126.

[6] A. Cieplý, E. Friedman, A. Gal, D. Gazda, J. Mareš, Phys. Lett. B 702 (2011) 402.

[7] A. Cieplý, E. Friedman, A. Gal, D. Gazda, J. Mareš, Phys. Rev. C 84 (2011) 045206.

[8] A. Ramos, E. Oset, Nucl. Phys. A 671 (2000) 481.

[9] B. Borasoy, R. Nissler, W. Weise, Eur. Phys. J. A 25 (2005) 79; Phys. Rev. Lett. 94 (2005) 213401.

[10] A. Cieplý, J. Smejkal, Eur. Phys. J. A 43 (2010) 191.

[11] CNS Data Analysis Center, http://gwdac.phys.gwu.edu

[12] A. Cieplý, J. Smejkal, Nucl. Phys. A 881 (2012) 115.

[13] A. Cieplý, J. Smejkal, Nucl. Phys. A 919 (2013) 46.

[14] A.M. Green, S. Wycech, Phys. Rev. C 71 (2005) 014001.

[15] M. Mai, P.C. Bruns, U.-G. Meissner, Phys. Rev. D 86 (2013) 015201.

[16] T. Waas, M. Rho, W. Weise, Nucl. Phys. A 899 (1997) 449.

[17] A. Cieplý, E. Friedman, A. Gal, D. Gazda, J. Mareš, Phys. Lett. B 702 (2011) 402; Phys. Rev. C 84 (2011) 045206.

[18] D. Gazda, J. Mareš, Nucl. Phys. A 881 (2012) 159.

[19] T. Yamazaki, Y. Akaishi, Phys. Lett. B 535 (2002) 70.

[20] N. V. Shevchenko, A. Gal, J, Mareš, Phys. Rev. Lett. 98 (2007) 082301; N. V. Shevchenko, A. Gal, J. Mareš, J. Révai, Phys. Rev. C 76 (2007) 044004.

[21] Y. Ikeda, T. Sato, Phys. Rev. C 76 (2007) 035203; Phys. Rev. C 79 (2009) 035201.

[22] T. Hyodo, W. Weise, Phys. Rev. C 77 (2008) 025212.

[23] S. Wycech, A. M. Green, Phys. Rev. C 79 (2009) 014001.

PoS(Bormio 2014)046

[24] M. Angelo et al. (FINUDA Collaboration), Phys. Rev. Lett. 94 (2005) 212303.

[25] T. Yamazaki et al. (DISTO Experiment), Phys. Rev. Lett 104 (2010) 132502.

[26] N. Barnea, A. Gal, E. Z. Liverts, Phys. Lett. B 712 (2012) 132.

[27] Y. Ikeda, H. Kamano, T. Sato, Prog. Theor. Phys. 124 (2010) 533.

[28] A. Dote, T, Hyodo, W. Weise, Nucl. Phys. A 804 (2008) 197; Phys. Rev. C 79 (2009) 014003.

[29] R. B. Wiringa, S. C. Pieper, Phys. rev. Lett. 89 (2002) 182501.

[30] Y. Kanada- En'yo, D. Jido, Phys. rev. C 78 (2008) 025212.

[31] E. Friedman, A. Gal, Nucl. Phys. A 881 (2012) 150.

[32] E. Friedman, A. Gal, Nucl. Phys. A 899 (2013) 60.

[33] M. Bazzi, et al., SIDDHARTA Collaboration, Phys. Lett. B 704 (2011) 113, Nucl. Phys. A 881 (2012) 88.

[34] J. Mareš, E. Friedman, A. Gal, Nucl. Phys. A 770 (2006) 84.

[35] T. Inoue, E. Oset, Nucl. Phys. A 710 (2002) 354; C. García-Recio, T. Inoue, J. Nieves, E. Oset, Phys. Lett. B 550 (2002) 47.

[36] Q. Haider, L. C. Liu, Phys. Rev. Lett. B 172 (1986) 257; L. C. Liu, Q. Haider, Phys. Rev. C 35 (1986) 1845; Q. Haider, L. C. Liu, Phys. Rev. C 66 (2002) 045208.

[37] A. Budzanowski, et al. (COSY-GEM Collaboration), Phys. Rev. C 79 (2009) 012201(R).

PoS(Bormio 2014)046